JOURNAL OF GEOPHYSICAL RESEARCH, VOL. 88, NO. C5, PAGES 2781-2791, MARCH 30, 1983

Norwegian Remote Sensing Experiment: Evaluation of the Nimbus 7 Scanning Multichannel Microwave Radiometer for Sea Ice Research

E. SVENDSEN,[1] K. KLOSTER,[2] B. FARRELLY,[1] O. M. JOHANNESSEN,[1] J. A. JOHANNESSEN,[1] W. J. CAMPBELL,[3] P. GLOERSEN,[4] D. CAVALIERI,[4] AND C. MÄTZLER[5]

An algorithm has been developed for estimating total and multiyear sea ice concentration from passive microwave and surface air temperature measurements. The algorithm was made for use with Nimbus 7 scanning multichannel microwave radiometer (SMMR) data. It is based on radiation physics and may thus easily be modified to suit other passive microwave instruments. A comparison between Nimbus 7 SMMR and aircraft microwave measurements indicates that estimates of total ice concentration are accurate to ±3% and those of multiyear ice concentration to ±10%. These accuracies are not valid during the melt season when the snow on the ice is wet. For the first time such a comparison of independent estimates has been performed to validate the capability of measuring sea ice coverage from space. The ability of the SMMR to follow moving patches of multiyear ice and of rain/wet snow areas has been demonstrated. From the concentration estimates the sharpness of the ice edge can be estimated. The need for accurate concentration estimates for reliable heat budget estimates in the Arctic is also discussed.

INTRODUCTION

The position of the ice edge and its movement, the concentration of the pack, and the ice types present are important parameters in sea ice dynamics/thermodynamics investigations as well as in climatological studies [*Pritchard*, 1980]. In these studies, remote sensing is potentially an important tool. Overviews of remote sensing of sea ice are reported by *Campbell et al.* [1976, 1978].

The scanning multichannel microwave radiometer (SMMR) on the Nimbus 7 satellite launched in 1978 was designed to measure the above mentioned parameters during all weather conditions [*Gloersen and Barath*, 1977]. As part of an evaluation program of the SMMR sensor capability in sea ice research, we carried out the Norwegian Remote Sensing Experiment (NORSEX) northwest of Svalbard during September/October 1979. One of the main objectives was to develop a SMMR ice algorithm, produce ice property maps, and evaluate this by comparison with simultaneous aircraft observations. To reach this objective, extensive surface observations were performed to determine the radiation properties of different ice types and water in the frequency range 5–100 GHz.

NORSEX included active and passive microwave aircraft observations. Their application to better understanding of the ice/ocean dynamics in the marginal ice zone is treated as a part of the NORSEX program. An overview of all the aspects of the NORSEX program is reported by the *NORSEX Group* [1982].

NIMBUS 7 SMMR OBSERVATIONS

Description of the SMMR Instrument

The Nimbus 7 SMMR is described in detail by *Gloersen and Barath* [1977]. It is a 10-channel radiometer receiving horizontally and vertically polarized microwave radiation at frequencies of 6.6, 10.7, 18, 21, and 37 GHz. The channels are designated 6V, 6H, 10V, etc., up to 37H. Radiation from the earth and its atmosphere is collected by a scanning reflector which covers areas out to 411 km from the satellite suborbital track. Its incidence angle on the earth is fixed at 50.2° (conical scan). The spatial resolution is defined as the field of view (FOV, also called footprint) which for different channels is primarily determined by antenna size and is inversely proportional to the frequency. FOV varies from about 30 km for 37 GHz to 150 km for 6.6 GHz, defined by the 3-dB beam width. Sampling is sufficiently closely spaced so that full resolution is achieved. The Nimbus 7 satellite was launched on October 24, 1978, and the SMMR is still operating (May 1982), so far exceeding its design lifetime of 1 year by a factor of 3.

Adjustment of Available SMMR Data

In each of the 10 SMMR channels, data are given as brightness temperatures measured within the footprints. Also given are coordinates on earth along the center of scan lines, making it possible to produce brightness temperature maps on a geographical grid. This is done by plotting values at the footprint centers using a high-resolution grid of 16 km × 20 km, followed by a filling-in operation using weighted spatial interpolation. From this material, ice property maps are produced by combining information in two or more channels, making use of a physical model.

It is found necessary to apply three adjustments to the brightness temperature maps in order to obtain proper alignment in space and proper temperature values before channel combination is performed. These three adjustments are as follows: (1) spatial adjustment relative to geographical grid, (2) low-pass spatial filtering of high-resolution (high-frequency) channels, and (3) linear adjustment of the brightness temperature.

The spatial adjustment accurate to within ±10 km was found by using the contours of Svalbard (Figure 5) on the brightness temperature maps [*NORSEX Group*, 1982].

A low-pass two-dimensional moving average filter is applied to the high-frequency channels to match the resolution of the lower frequencies used in channel combination.

Passive microwave measurements of radiation from a

[1] Geophysical Institute, University of Bergen, Norway.
[2] Christian Michelsens Institute, Bergen, Norway.
[3] United States Geological Survey, Tacoma, Washington 98416.
[4] Goddard Space Flight Center, Greenbelt, Maryland 20771.
[5] Institute of Applied Physics, University of Bern, Bern, Switzerland.

Paper number 2C1378.
0148-0227/83/002C-1378$05.00

target are expressed as brightness temperatures in kelvins. The available brightness temperatures are obtained from the measured raw digital radiometric data by use of the prelaunch laboratory calibration and additional corrections for polarization mixing (both dependent and independent of scan angle) discovered in orbit [*Gloersen et al.*, 1981].

Transformation of radiometric data to calibrated brightness temperatures by using prelaunch data and polarization demixing is generally difficult. Our algorithm for retrieving geophysical parameters is dependent on well-calibrated values for brightness temperatures. Therefore additional in-orbit calibration over known radiators, open ocean (cold calibration point), and first-year sea ice (warm calibration point) is performed in conjunction with measured and modeled atmospheric corrections. For calm seawater the emission is well known from both theoretical computations and from NORSEX measurements [*NORSEX Group*, 1982]. This emission, adjusted for atmospheric effects (described in the next section), is compared with SMMR measurements over a suitable open water area between Svalbard and Greenland on days with very calm wind conditions. Ship measurements and weather maps indicated winds less than 2 m/s. A similar calibration over 100% first-year ice cover in Baffin Bay [*Gloersen et al.*, 1981] showed good agreement with the prelaunch blackbody calibration. This gives a warm and a cold calibration point for each channel, and a linear interpolation between these points is done to correct all the available brightness temperatures.

With these three adjustments made, a new set of calibrated brightness temperature maps is produced, suitable for computing geophysical parameters by channel combination.

NORSEX Ice Algorithm

Radiation Model

The radiation model used is composed of two main parts, a model of the surface and a model of the atmosphere above. Also, radiation from free space gives a minor contribution.

The sea ice is in reality a three-dimensional structure where microwave radiation is emitted and reflected in a complex way somewhere between the surface and the bottom, which is water at 272 K. When we define an 'effective' emissivity ε_{eff} for this material treated as a two-dimensional surface, it is related to an 'effective' temperature T_{eff} in the ice such that the product, called 'emitted brightness,' is the net radiation emitted:

$$T_E = \varepsilon_{\text{eff}} T_{\text{eff}} \tag{1}$$

It is what a radiometer would detect immediately above the surface without radiation from above. The situation is still more complex for a mixture of water and ice. The radiation model expressing the radiation T_H sensed at satellite height

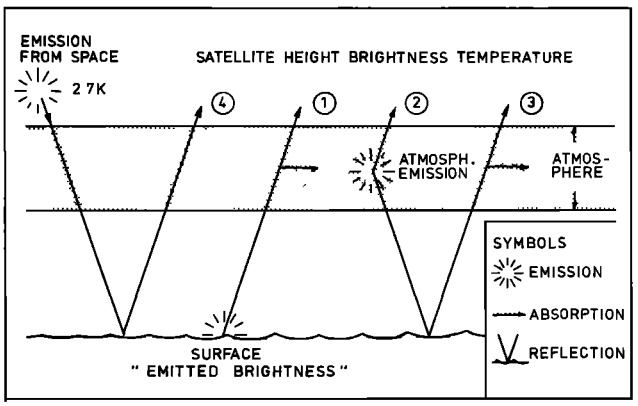

Fig. 1. Illustration of the four terms in the radiation model.

is composed of four terms (see Figure 1): (1) emitted brightness from the surface seen through the atmosphere, (2) upwelling radiation from the atmosphere, (3) downwelling atmospheric radiation reflected at the surface and transmitted back through the atmosphere, and (4) radiation from space after reflection from the surface.

$$T_H = \underset{1}{\varepsilon_{\text{eff}} T_{\text{eff}}(1 - \tau_a)} + \underset{2}{\delta T_a \tau_a} + \underset{3}{(1 - \varepsilon_{\text{eff}})\delta T_a \tau_a (1 - \tau_a)} + \underset{4}{(1 - \varepsilon_{\text{eff}}) T_{\text{sp}}} \tag{2}$$

Here, τ_a is total atmospheric opacity (optical depth), and T_{sp} is the temperature of free space, approximately 2.7 K; δT_a is the weighted average atmospheric temperature in the lower troposphere [*Gloersen et al.*, 1978; *Shutko and Granov*, 1982].

This equation is a simplified version of the more accurate equation [*Gloersen and Barath*, 1977, equation 1]. Since τ_a is small, the approximation $e^{-\tau_a} = 1 - \tau_a$ is used, and a term $T_{\text{sp}} 2\tau_a$ is neglected. Furthermore, downwelling and upwelling atmospheric radiation have been assumed to be equal. The first and dominant term of (2), $\varepsilon_{\text{eff}} T_{\text{eff}}$, is replaced by T_E (equation (1)). In the remaining correction terms, ε_{eff} is written as T_E/T_{eff}, and T_{eff} is approximated as $\beta^{-1} T_a$ where β is a constant close to 1. From the procedure we arrive at the following equation for computing T_E from T_H:

$$T_E = (T_H - 2\delta T_a \tau_a + \delta T_a \tau_a^2 - T_{\text{sp}}) \div [1 - \tau_a - \beta\delta(\tau_a - \tau_a^2) - \beta(T_{\text{sp}}/T_a)] \tag{3}$$

Values for τ_a in atmospheres with T_a = 270 K (Subarctic winter) and T_a = 250 K (Arctic winter) are given by *Reeves* [1975] and listed in Table 1. The Subarctic winter values compare well with the mean opacities measured during NORSEX (Table 2). However, large variations occurred in

TABLE 1. Opacities (Optical Depths) for Two Model Atmospheres Used in the Radiation Model

	Frequency for Subarctic Winter, GHz					Frequency for Arctic Winter, GHz				
	6.6	10.7	18	21	37	6.6	10.7	18	21	37
Oxygen τ_0	0.011	0.011	0.015	0.022	0.034	0.011	0.011	0.015	0.022	0.034
Water vapor τ_W	0.000	0.001	0.006	0.016	0.012	0.000	0.000	0.003	0.008	0.006
Liquid water τ_1	0.001	0.003	0.009	0.012	0.038	0.000	0.001	0.004	0.006	0.019
Total zenith τ_2	0.012	0.015	0.030	0.050	0.084	0.011	0.012	0.022	0.036	0.059
Total 50° τ_a	0.019	0.023	0.047	0.078	0.130	0.017	0.019	0.034	0.056	0.091

For Subarctic winter, T_a = 270 K, W (water vapor) = 0.4 cm, and L (liquid water) = 0.02 cm. For Arctic winter, T_a = 250 K, W = 0.2 cm, and L = 0.01 cm.

TABLE 2. Model Atmosphere Zenith Opacities (Optical Depths) Compared With Measured Mean NORSEX Values

	Frequency, GHz			
	4.9	10.4	21	36
Subarctic winter model atmosphere	0.011	0.015	0.050	0.082
Arctic winter model atmosphere	0.010	0.012	0.036	0.058
NORSEX ice edge fall 1979 atmosphere	0.011	0.015	0.062	0.073

the measurements [*NORSEX Group*, 1982], indicating that the opacities vary considerably with conditions other than T_a, e.g., clouds. For surface temperatures other than 270 K and 250 K, a linear interpolation is made between the values in Table 1 to arrive at atmospheric opacity values.

The parameters β and δ are given the values of 0.95 and 0.9 in actual computations. These values are sufficiently good approximations, considering the uncertainties already present in the values for τ_a.

The emitted brightness T_E from a surface consisting of three components is now considered. The three components are as follows: (1) seawater, effective temperature 272 K, emissivity ε_W, and concentration C_W, (2) multiyear ice, effective temperature T_{ice}, emissivity ε_M, and concentration C_M, and (3) first-year ice, effective temperature T_{ice}, emissivity ε_F, and concentration C_F. Concentrations are defined as area fractions, thus:

$$1 = C_M + C_F + C_W \tag{4}$$

The emitted brightness temperature from this three-component surface is assumed to be the sum of individual emitted brightness temperatures, weighted by the concentrations:

$$T_E = \varepsilon_{\text{eff}} T_{\text{eff}} = C_M \varepsilon_M T_{\text{ice}} + C_F \varepsilon_F T_{\text{ice}} + C_W \varepsilon_W 272 \tag{5}$$

The emissivities ε_M, ε_F, and ε_W have all been measured by shipborne radiometer in the NORSEX experiment near the ice edge. However, comparison with aircraft measurements indicated that these emissivities are also representative for the ice further into the pack. The emissivity ε_W for seawater agrees closely with theoretical values computed from dielectric constants [*NORSEX Group*, 1982].

As T_{ice} is not readily measured, we need a relation between T_{ice} and the surface temperature which is assumed to be equal to the surface atmospheric temperature T_a. On the basis of the reasoning that T_{ice} is found somewhere between the surface and the underlying water, we have

$$T_{\text{ice}} = \alpha T_a + (1 - \alpha)272 \tag{6}$$

To estimate α, the variation of T_E (calculated from the adjusted SMMR measurements) of an area north of Ellesmere Island has been studied in relation to changes in surface air temperature measured from ice drifting buoys. The area marked BC, the location of the buoys, and also their measurements are shown in Figure 2. This area is chosen since it is known to have a very high and constant concentration of multiyear ice. A gradual decline of T_E as the surface air temperature in the area decreases from 265 K to 250 K is seen. Assuming that no great variation in the surface composition takes place, a value for $\partial T_E/\partial T_a$ around 0.3 is observed for all frequencies. Combining (5) and (6) and taking the derivative $\partial/\partial T_a$, assuming the emissivities and α are weak functions of T_a, this gives a rough estimate of $\alpha \approx 0.4$. Comparing this with NORSEX temperature measurements of multiyear ice covered with snow indicates that the temperature near the snow/ice interface represents the effective temperature T_{ice}. By correct choice of two SMMR channels and knowledge of the surface air temperature, C_M and C_F can be computed from (3)–(6). No attempt is made to explicitly compute the atmospheric opacity (τ_a) or the ice surface temperature. The accuracy of these parameters if computed over a complex ice surface will be questionable, because a relatively small uncertainty in brightness temperature will have a large effect on the estimates of these parameters.

Selection of SMMR Channels

From the surface-measured emissivity spectra of multiyear ice, first-year ice, and water [*NORSEX Group*, 1982] shown in Figure 3, it is seen that because of the large difference between multiyear ice and first-year ice at 37 GHz, this is the best choice of frequency to separate the two ice types. Furthermore, the spectra indicate that to separate ice from water, one of the lower frequencies must also be used, giving the best accuracy but unfortunately the worst spatial resolution for the lowest frequency.

Comparison of mean (in space and time) brightness temperature spectra measured in the area BC north of Ellesmere Island with spectra in an area (area AA in Figure 2) well into the pack north of Svalbard shows unexplained variations in the horizontally polarized channels. Furthermore, the horizontal spectra from area BC lie 5–25 K higher than calculated on the basis of concentrations which have been estimated from the vertical spectra. Similar properties are seen in some of the aircraft data and in the surface measurements and have also been observed by other groups [*Skou*, 1980]. We therefore exclude all horizontal channels when computing multiyear and first-year ice concentrations.

At present, we are not sure what causes the horizontal polarization excess. However, an increase in the horizontally polarized surface radiometric measurements of multiyear ice was observed when the 15- to 20-cm-thick snow cover containing several thin ice layers was trampled. This indicates that changes in the small-scale structure of the snow may cause the excess observed from the SMMR. Another possibility is the 'large-scale' ice surface roughness. Area BC north of Ellesmere Island is known to be a heavily ridged area, which means that the measurements represent emission at a variety of incidence angles. This could also cause the excess and increased variability of the horizontally polarized signals observed from the satellite.

On the basis of this information the combination of 10V/37V is chosen for estimates of C_M and C_F, but comparable estimates from the combination 18V/37V are also made to give better spatial resolution.

Algorithm

The algorithm computes ice concentrations C_M for multiyear and C_F for first-year ice. Input is the available SMMR brightness values from two channels, 10V (or 18V) and 37V, and a value for the surface air temperature over dense pack ice, T_p. In actual use, T_p averaged over a few days is derived from automatic ice buoys drifting within the ice (Figure 2).

The algorithm consists of the following computational steps:

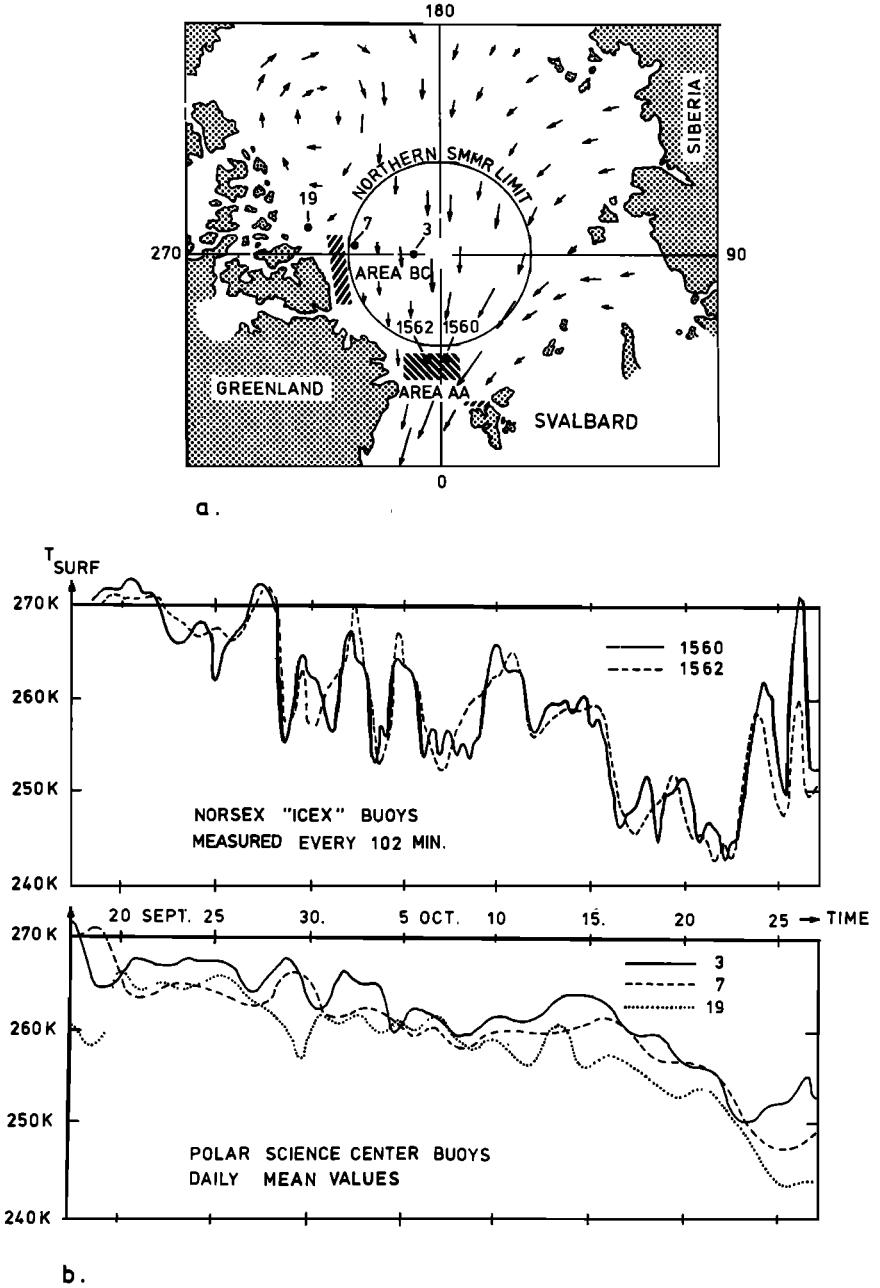

Fig. 2. Map of the polar ocean and temperature during the NORSEX experiment. (*a*) Location of selected areas AA and BC and of five temperature-measuring buoys with associated buoy numbers. Arrows indicate annual ice drift. (*b*) Surface temperature measured by buoys.

1. The available SMMR data are adjusted as earlier explained to give 'calibrated' brightness temperatures T_H at satellite height.

2. An initial transformation of T_H to emitted brightness T_E is performed using an atmosphere corresponding to T_p ($T_a = T_p$).

3. By solving (4)–(6) (using two channels gives two equations with two unknowns), initial concentrations are found using $T_a = T_p$.

4. A refined atmosphere (τ_a and T_a) is found by using initial total ice concentration from step 3 to interpolate between surface temperature over water (T_a = 272 K) and over 100% ice ($T_a = T_p$). The refined opacities are then found from T_a.

5. Steps 2 and 3 are repeated using the refined atmosphere, arriving at final values for the concentrations.

After concentrations are computed, measured and computed emitted brightness of the 10H (or 18H) channel can be found from (3) and (5), respectively. The difference T_E (measured) − T_E (computed from concentrations) is a measure of the horizontal polarization excess.

Ice Maps

Two days, October 11 and September 29, have been chosen to show the results from the NORSEX ice algorithm used on the available SMMR data. Figures 4 and 5 show the total and multiyear ice concentrations on October 11, based on the 10V/37V and 18V/37V channel combination with

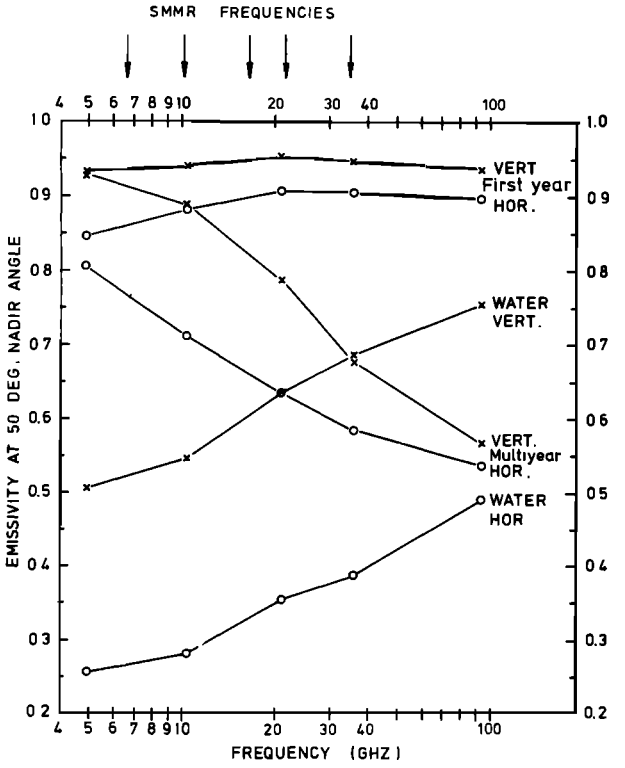

Fig. 3. Emissivities of calm seawater, multiyear ice, and first-year ice as a function of frequency measured during NORSEX.

spatial resolutions of 90 km and 60 km, respectively. The somewhat higher spatial resolution from the 18V/37V combination is seen especially in the ice edge region where the gradient of total concentration going from open water into the pack is sharper than for the 10V/37V combination. Apart from this, the results look fairly similar. The well-known low-concentration area near Greenland is seen [*Koch*, 1945]. Also shown is the best estimate of the position of the ice edge (accuracy ±10 km [*NORSEX Group*, 1982]) taken from the maximum gradient of the 37H channel which coincides very well with the 45% total ice concentration isoline (not shown in the figures). Similar results for September 29 are shown in Figures 6 and 7. Notice the patch of high multiyear ice concentration occurring on both days. The movement of this patch will be discussed in a later section. On both days, flight tracks are shown, and a comparison between the aircraft and SMMR results along these lines is discussed in the next section.

Comparison of Aircraft- and Satellite-Measured Ice Concentrations

During NORSEX, several flights were performed with the NASA C-130 aircraft carrying several microwave instruments. Data from the nadir-looking stepped frequency microwave radiometer (SFMR) used at 6.6 GHz and the multifrequency microwave radiometer (MFMR) with a 50° viewing angle make it possible to estimate total ice and multiyear ice concentrations along the flight lines. This is compared with the computed SMMR ice concentrations along the same lines. These estimates are completely independent except for the assumption that (5) is valid.

Only two flights, September 29 and October 10, 1979 (Figures 4 and 6), went far enough into the ice so that comparison could be made (because of the large field of view, the SMMR cannot measure ice concentration accurately near the ice edge), and unfortunately the MFMR was only run on October 10.

In the comparison one must remember that the aircraft measurements represent a line through the large SMMR footprints. To account for some of this, a low-pass filter (80-km running mean) is used on the aircraft data.

The model used on the aircraft data is based on (4) and (5), where $\varepsilon_M T_{\text{ice}}$, $\varepsilon_F T_{\text{ice}}$, and $\varepsilon_W 272$ are substituted by aircraft-measured mean brightness temperatures of 100% multiyear ice, first-year ice, and water. By this procedure an absolute calibration of the aircraft data is not necessary. Unfortunately, the MFMR 37 GHz channels malfunctioned, so the 21H channel had to be used in addition to the 6.6-GHz SFMR.

The 100% signatures based on 200–300 samples of each target type are listed in Table 3 together with the standard deviations. The targets were identified by continuous aerial

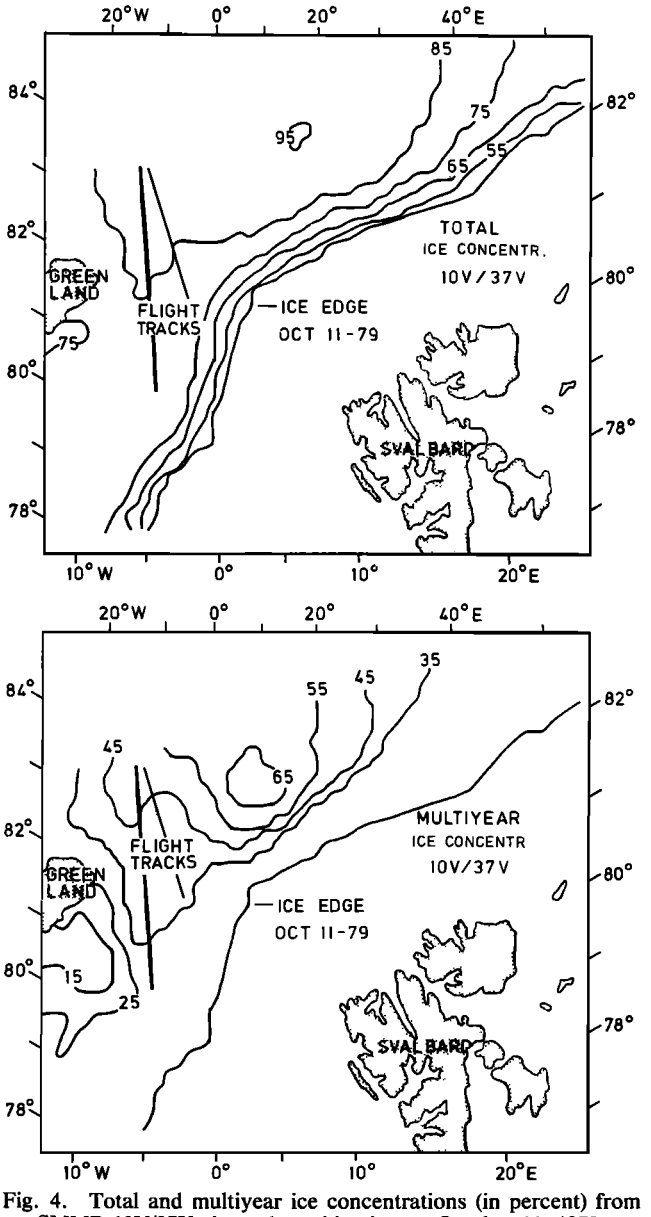

Fig. 4. Total and multiyear ice concentrations (in percent) from SMMR 10V/37V channel combination on October 11, 1979.

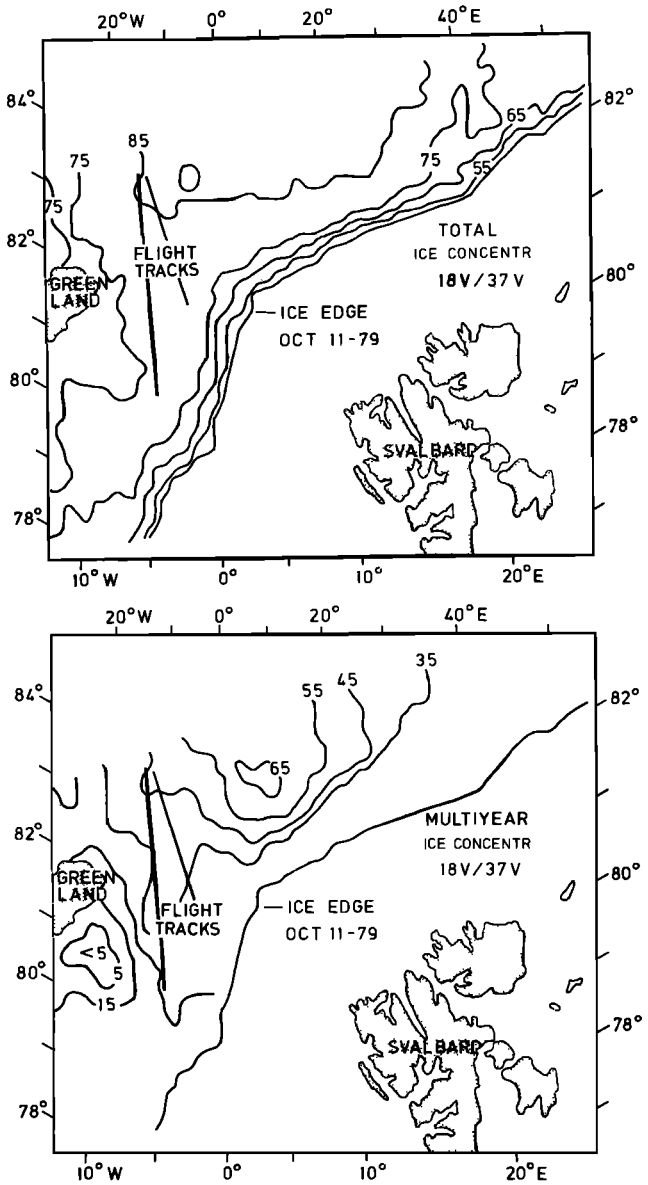

Fig. 5. Total and multiyear ice concentrations (in percent) from SMMR 18V/37V channel combination on October 11, 1979.

photography. The standard deviations are mainly caused by the complexity of the ice/snow itself, but also include possible errors in the instruments and variability of the atmosphere. This means that from the standard deviations, the uncertainty of the aircraft concentration estimates can be computed, being a function of the amount of different ice types present. For the worst case, if near 100% multiyear ice is present, the uncertainty of total ice concentration will be ±5%, and that of multiyear ice concentration ±15%.

Figures 8 and 9 show comparisons along two lines flown on October 10, while the SMMR measured 18 hours later on October 11. Total ice concentration and multiyear ice concentration are shown, and the difference between these two is the concentration of first-year ice. A very good fit is seen between the SMMR 10/37 and the aircraft estimates of total ice concentration with a mean difference of 0.5 ± 2.5%. For the concentrations present, the absolute accuracy of the aircraft total ice concentration estimates is ±3%. The difference between the SMMR 18/37 and the aircraft total ice concentrations is −3.5 ± 2.0%, indicating that with this channel combination the SMMR estimates are a few percent too low. The reason for this might be that an error in the SMMR calibration points or the atmospheric correction gives a greater effect on this channel combination than the 10/37 combination.

The multiyear ice estimates show a mean difference between SMMR 10/37 and aircraft of −4 ± 6%, and between SMMR 18/37 and aircraft of −8 ± 6%. The absolute accuracy of the aircraft multiyear ice concentration is estimated to ±10%.

Figures 10 and 11 show similar comparisons along two lines flown on September 29. Now the time difference is only 4–6 hours between the aircraft and the satellite sampling. On this day, only the SFMR was on, and therefore no multiyear ice concentration estimates could be done from the aircraft. The uncertainty in the aircraft total ice concentration esti-

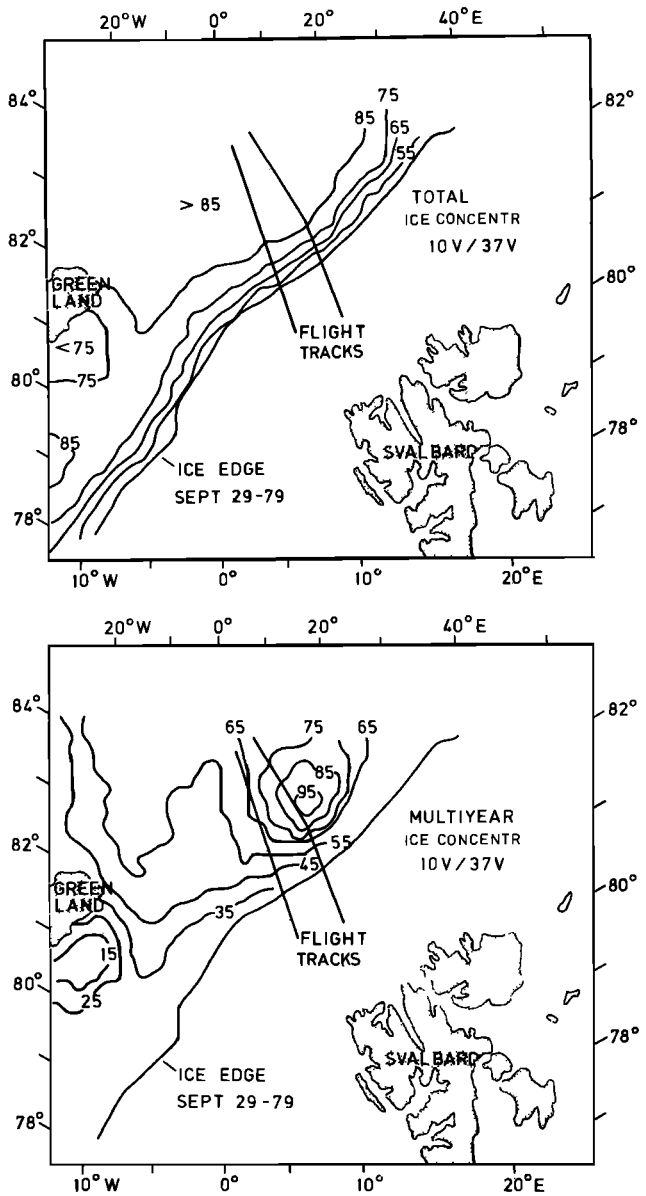

Fig. 6. Total and multiyear ice concentrations (in percent) from SMMR 10V/37V channel combination on September 29, 1979.

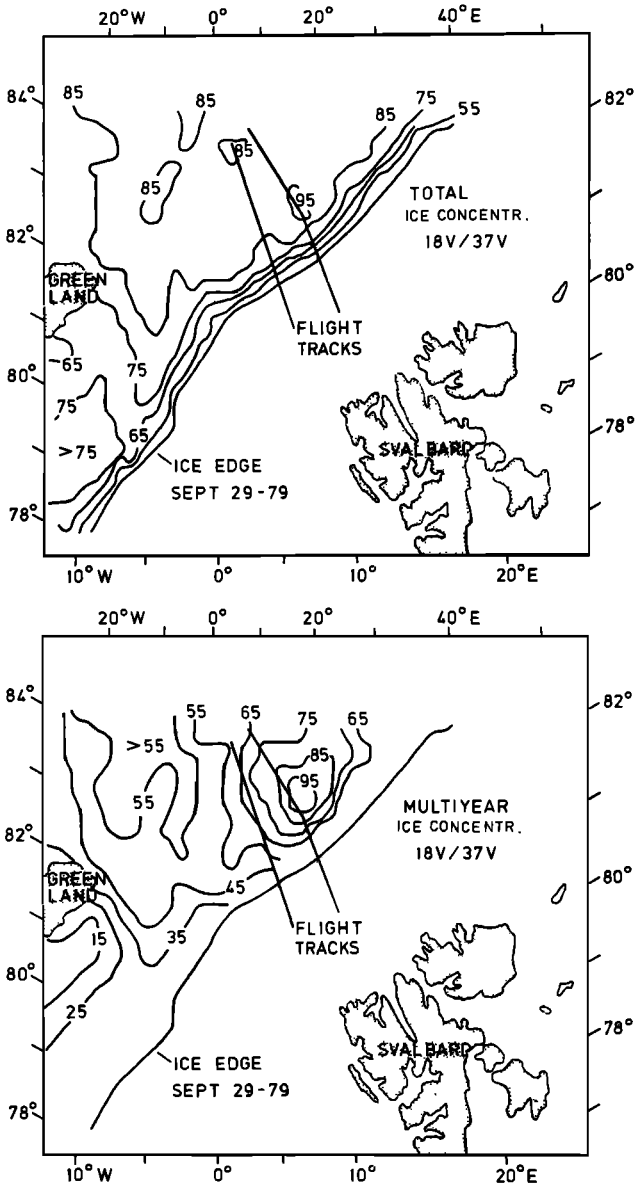

Fig. 7. Total and multiyear ice concentrations (in percent) from SMMR 18V/37V channel combination on September 29, 1979.

mates has also increased to ±6%. From the figures it is seen that the mean difference between SMMR and aircraft is within this uncertainty. In these figures the results in the vicinity of the ice edge are also shown. It is seen that the position of the ice edge taken from nonaveraged aircraft data coincides approximately with half the SMMR total ice concentration inside the edge. Also seen is that the 18/37 combination gives the expected improvement in spatial resolution.

This comparison has some limitations. First, it is not possible to do two-dimensional low-pass filtering of the aircraft data to match the SMMR FOV. Second, the comparison is done in a limited region and within a limited time of the year. Consequently, any general statement on the accuracy of SMMR ice concentration estimates is avoided. However, the principles underlying the algorithm are completely general, and evaluation of the algorithm on a larger data set is in progress.

The NORSEX ice algorithm uses surface measurements of air temperature in conjunction with a modeled atmosphere as input in the radiation equation. With present close monitoring of the Arctic Ocean with temperature-measuring automatic stations, data for temperature input are largely available. NORSEX emissivities have been used [*NORSEX Group*, 1982], and they seem to be appropriate for this area and the time under study, but may of course be refined by future investigations. For instance, wet snow on the ice will change the multiyear emissivities considerably.

Using the 10V/37V channel combination, our estimates of total ice concentration from the SMMR are shown to be accurate to ±3%, and the multiyear ice concentration accurate to ±10%. If large areas of very thin ice are present or melt ponds exist on the ice, the uncertainties of both total and multiyear ice concentration will be larger. Moreover, if the snow on the multiyear ice is wet, the multiyear ice will be estimated as first-year ice.

APPLICATION OF SMMR RESULTS

Ice Edge

The *NORSEX Group* [1982] showed that the SMMR could detect a well-defined ice edge to an accuracy of ±10 km. A 40-day comparison of the ice edge north of Svalbard estimated from the SMMR and the ice edge estimated by the Norwegian Meteorological Institute (MI) by use of Tiros, NOAA, and sporadic aircraft and ship observations showed that MI's estimates had a standard deviation of about 40 km relative to the SMMR estimates. Since clouds very often are present in the ice edge region, this means that passive microwave remote sensing can be used to improve the present ice edge mapping.

It might be of interest to know the structure of the edge, whether the edge is sharp or loose. On October 23, two lines have been chosen on the concentration map (Figure 12), one (profile C-D) perpendicular to a sharp edge and the other (profile A-B) perpendicular to an 'edge' with alternating leads and ice floes. The structure of the edge indicated by the temperature profiles (Figure 12) is taken from a map produced one day earlier from the thermal infrared (IR) channel of the advanced very high resolution radiometer (AVHRR) instrument in the NOAA 6 satellite. The SMMR profiles are also shown in Figure 12. Note that the spatial resolution of the AVHRR profiles and the SMMR profiles is 1 km and 60 km, respectively. The filtered AVHRR curve shown by the dashed line has a resolution roughly comparable to the SMMR curves. It is seen that the loose edge gives a much more gradual SMMR profile than the sharp edge, which essentially shows a 'step response' as in Figures 10 and 11. The SMMR profile of the loose ice edge is stretched out approximately 60 km more than the other, indicating that the transition from open water to the dense ice pack in the loose region is on average approximately 60 km. This compares well with what is seen from the IR picture. Since the

TABLE 3. Airborne Measurements of Brightness Temperature From 100% Calm Water, First-Year Ice, and Multiyear Ice

Airborne (C-130) Sensor	Water	First-Year Ice	Multiyear Ice
SFMR, 6.6 GHz	106 ± 0	244 ± 2	229 ± 5
MFMR, 21 GHz H	110 ± 1	253 ± 2	190 ± 5

Values are in kelvins.

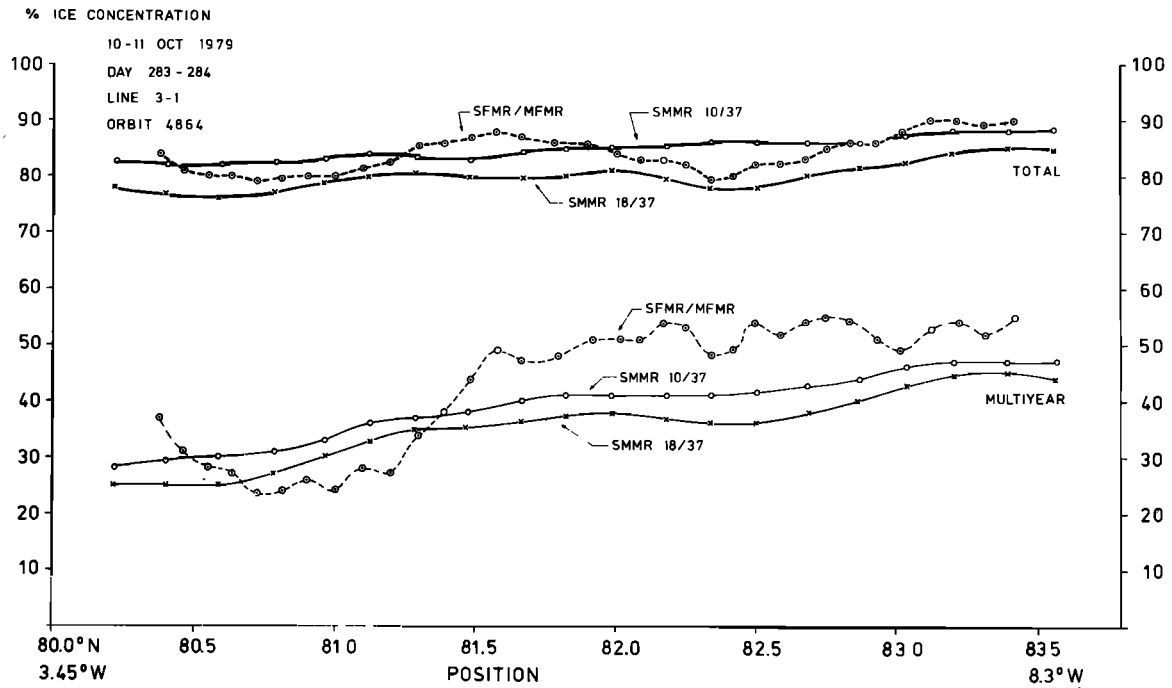

Fig. 8. Comparison of aircraft (SFMR/MFMR) and satellite (SMMR) estimates of ice concentrations, October 10–11, 1979, along westerly track (Figure 4).

multiyear ice profile starts to increase further north than the total ice profile, this indicates that the outermost ice is mainly first-year ice. Note that the crossover of multiyear and total ice concentration in Figure 12 is not significant.

Detection of Moving Ice and Atmospheric Features by SMMR

During the 40-day period, September 17 through October 27, for which SMMR data are available, a patch of high multiyear ice concentration (Figures 4 to 7) is seen on most of the maps. The center position of the patch is plotted in Figure 13 for all days it could be confidently measured, together with the synoptic position of two of our drifting buoys. A very good correlation is seen between the SMMR-measured ice drift and the buoys.

On five days, September 17, 19, 21, and 27 and October 27, this multiyear ice signature disappears partly or completely and is replaced by first-year ice signature. On these

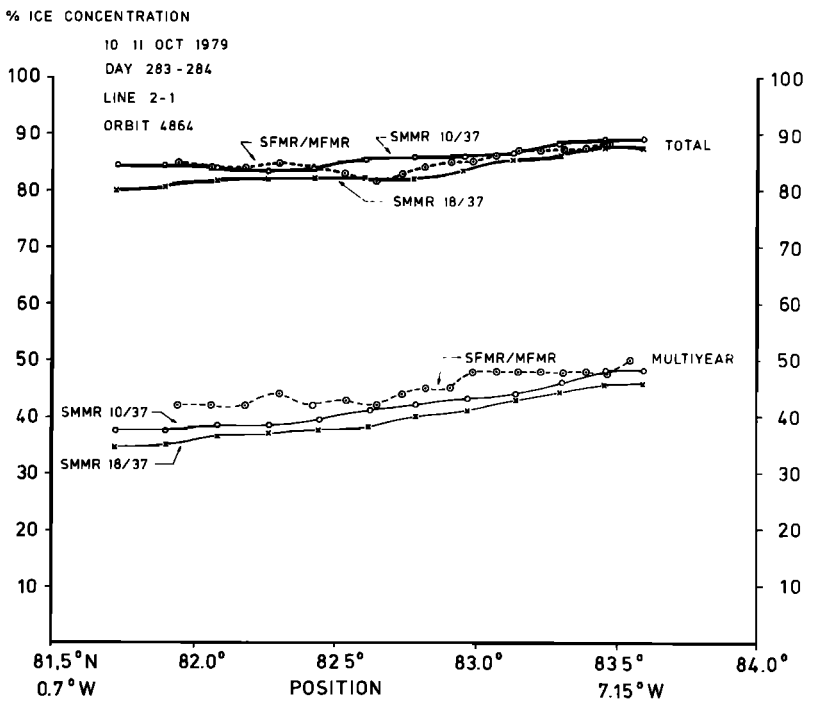

Fig. 9. Comparison of aircraft (SFMR/MFMR) and satellite (SMMR) estimates of ice concentrations, October 10–11, 1979, along easterly track (Figure 4).

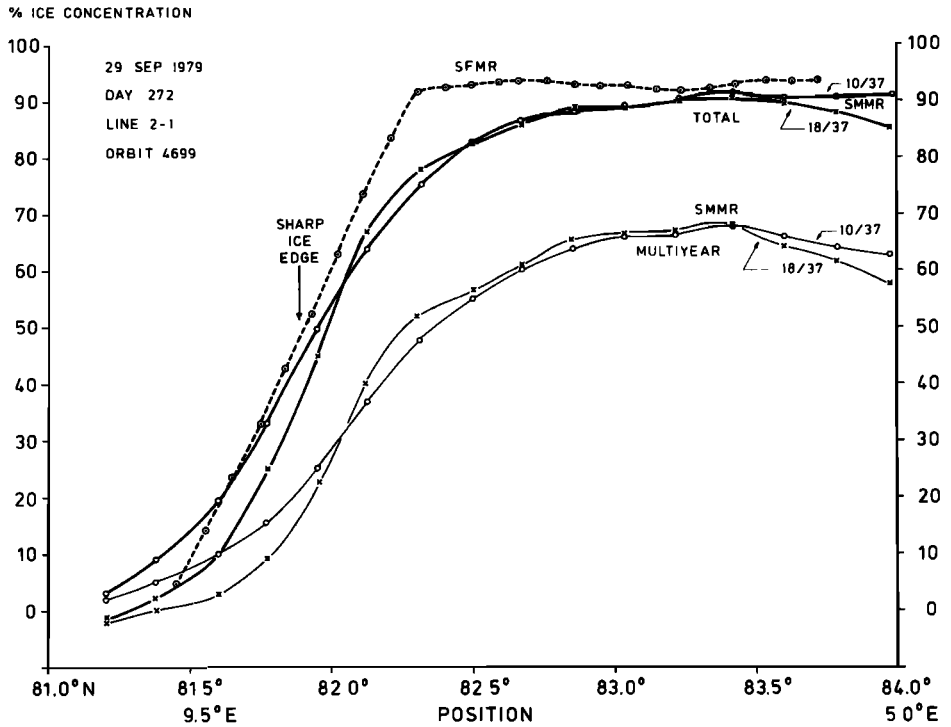

Fig. 10. Comparison of aircraft (SFMR) and satellite (SMMR) estimates of ice concentrations, September 29, 1979, along westerly track (Figure 6).

and only on these days, buoy 1560 measured air temperature above 270 K (Figure 2). Our conclusion is that rain and/or wet snow is obscuring the multiyear ice signature on these occasions. The total ice concentration is affected very little, and the ice edge seems to be well defined on all days.

On two days during the period, the obscuring first-year ice signature has the form of a nearly circular patch with a diameter of 100–150 km. Since we suspected this signature to be caused by the atmosphere, its movement has been measured on maps spaced two satellite revolutions, or 3.3 hours, apart. On September 21, no movement was observed, corresponding well to a wind speed less than 1 m/s measured

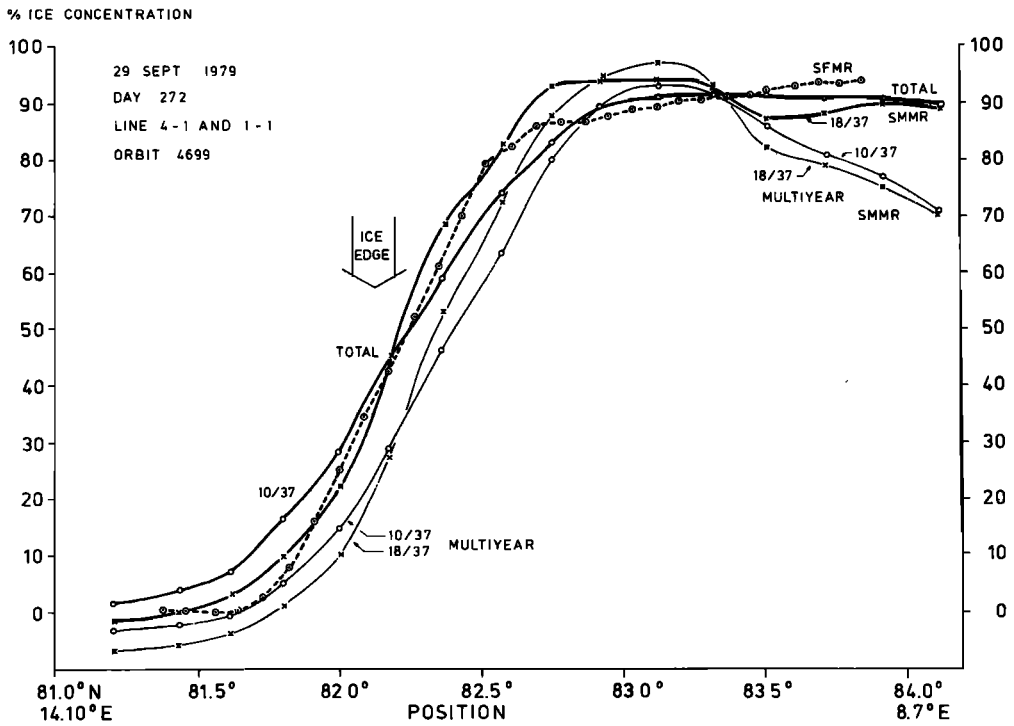

Fig. 11. Comparison of aircraft (SFMR) and satellite (SMMR) estimates of ice concentrations, September 29, 1979, along easterly track (Figure 6).

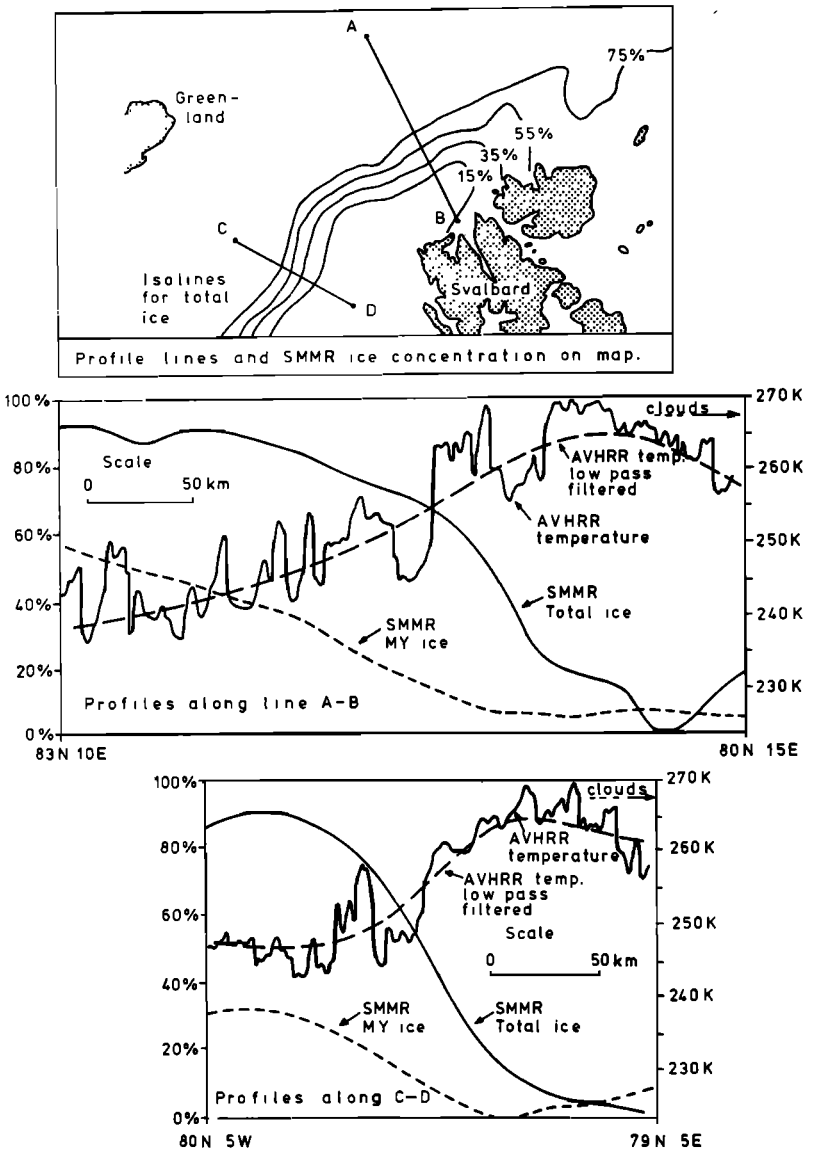

Fig. 12. Profiles of SMMR ice concentrations across the ice edge (60-km resolution) on October 23 and of AVHRR temperature (1-km and 60-km resolution) on October 22, 1979, along line AB and line CD.

from the icebreaker *Polarsirkel* situated 120 km to the south. On September 27, the 'wet' patch was moving to the west at approximately 6 m/s, again corresponding well to a ship-measured wind of 7 m/s in the same direction.

In summary, it has been possible to measure total ice concentration during the whole NORSEX period with varying air temperature from 272 K to 243 K. On five days the ice type signatures are obscured by rain and/or wet snow over a relatively small area, making multiyear ice look like first-year ice. This is not unexpected at this time of the year, and this problem will probably decrease with the advance of the cold season and also with increasing distance from the ice edge. Both mean ice movements and atmospheric movements can be detected by the SMMR whenever the ice or atmosphere causes well-defined signatures similar to the multiyear and wet patches.

Heat Budget

The accuracies of our concentration estimates should be compared with the accuracies necessary for reliable heat budget estimates. *Maykut* [1978] has a good description of this subject, and as an example his numbers from March are used to calculate the relative change in the net heat loss to the atmosphere with respect to change in total ice concentration. March was chosen, as the oceanic heat loss is large for this month. It is assumed that only water and multiyear ice are present and that the atmospheric boundary layer is determined by the heat balance over the thick ice. If, for example, the actual ice concentration is 95% and the concentration estimate is 3% off, the estimate of net heat loss will be off by 50%. If, instead, the actual ice concentration is 80% and the concentration estimate is off by the same 3%, the estimate of net heat loss is only off by 15%. In reality the error will be slightly less, since at lower ice concentration the atmospheric boundary layer will be significantly affected by the amount of open water. This means that for high total ice concentration, especially during the cold season, very accurate estimates of the ice concentration are needed for good estimates of the heat exchange.

It is also found that when the total ice concentration is

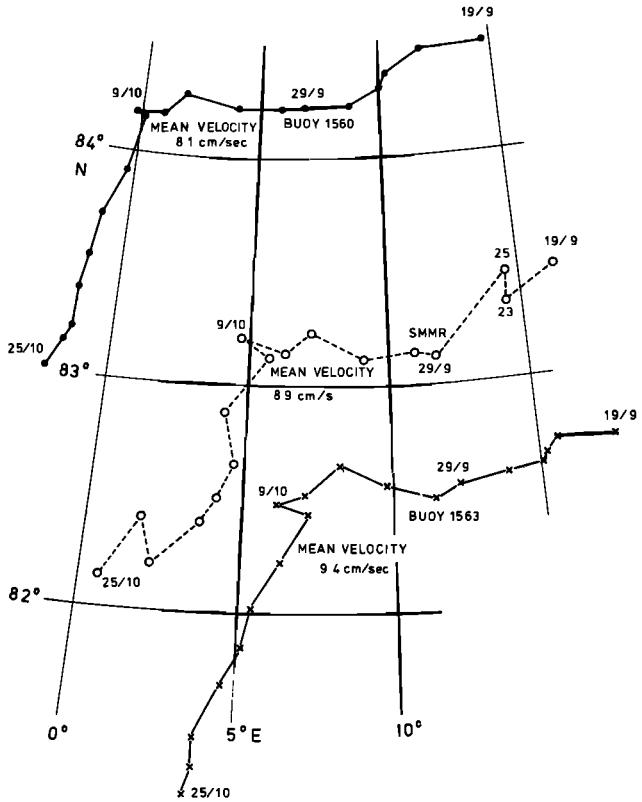

Fig. 13. Comparison of ice movement measured from SMMR (patch of multiyear ice) with drifting buoys on the ice.

high, it is important to know the amount of very thin ice in order to make good estimates of the heat exchange. In our SMMR algorithm we only assume thicker first-year ice, multiyear ice, and water present in the area. If very thin ice also is present, this will be interpreted partly as thicker ice and partly as water. This will to a certain degree balance with respect to heat exchange estimates, but obviously more studies are needed for better estimates of the very thin ice.

Even if the accuracies of the SMMR results fall short of the requirements for the ultimate in heat budget estimates over the Arctic, such estimates based on SMMR data would be a vast improvement over any other existing technique.

Conclusions

An independent comparison with aircraft radiometric measurements indicates that the scanning multichannel microwave radiometer (SMMR) estimates of total ice concentration are accurate to ±3% and those of multiyear ice concentration to ±10% with spatial resolution of 90 km. Better spatial resolution (60 km) can be obtained with slightly less accurate concentration estimates. The concentration maps presented have a geographical positioning accuracy of ±10 km.

More aircraft measurements are needed to check the validity of the estimates at different times of the year and in different regions. It seems that when wet snow occurs on the ice, the total concentration estimates are little affected while the multiyear ice will be interpreted as first-year ice.

From the concentration estimates it is possible to estimate the width of the ice edge transition zone from open water to dense pack ice. Some indication of which ice type is present in this zone is also possible.

The ability of the SMMR to detect moving patches of multiyear ice suggests the possibility of using the SMMR for ice kinematic studies. There is little doubt that such spaceborne microwave radiometer measurements can contribute to improve present heat budget estimates over the Arctic.

Acknowledgments. The NORSEX program was funded by the University of Bergen, Norway; The Royal Norwegian Council for Scientific and Industrial Research/Space Activity Division; National Aeronautic and Space Administration, United States; Office of Naval Research, United States (grant 0014-80-G-0003); U.S. Geological Survey; and Scientific Affairs Division of NATO (grant 9-4-02-SRG.19).

References

Campbell, W. J., W. F. Weeks, R. O. Ramseier, and P. Gloersen, Geophysical studies of floating ice by remote sensing, *J. Glaciol. 15*, 305–327, 1976.

Campbell, W. J., et al., Microwave remote sensing of sea ice in the AIDJEX Main Experiment, *Boundary Layer Meteorol., 13* (1–4), 309–337, 1978.

Gloersen, P., and F. T. Barath, A scanning multichannel microwave radiometer for Nimbus-G and Seasat-A. *IEEE J. Oceanic Eng., OE-2* (2), 172–178, 1977.

Gloersen, P., H. J. Zwally, A. T. Chang, D. K. Hall, W. J. Campbell, and R. O. Ramseier, Time dependence of sea-ice concentration and multi-year ice fraction in the Arctic basin, *Boundary Layer Meteorol., 13*, 339–359, 1978.

Gloersen, P., D. J. Cavalieri, and J. A. Gatlin, Nimbus-7 scanning multichannel microwave radiometer, in orbit performance appraisal, paper presented at International Geoscience and Remote Sensing Symposium (IGARSS'81), Inst. of Electr. and Electron. Eng., Washington, D. C., 1981.

Koch, L., The East Greenland Ice, *Medd. Groenl., 130* (3), 374 pp., 1945.

Maykut, G. A., Energy exchange over young sea ice in the central Arctic, *J. Geophys. Res., 83*, 3646–3658, 1978.

Norwegian Remote Sensing Experiment (NORSEX) Group, The Norwegian Remote Sensing Experiment (NORSEX) in the marginal ice zone north of Svalbard, Geophys. Inst., Univ. of Bergen, Bergen, Norway, submitted to *Science*, 1982.

Pritchard, R. S. (Ed.), Sea ice processes and models, in *Proceedings of the Arctic Ice Dynamics Joint Experiment/International Commission on Snow and Ice Symposium 1977*, University of Washington Press, Seattle, Wash., 1980.

Reeves, R. G. (Ed.), *Manual of Remote Sensing*, American Society of Photogrammetry, Falls Church, Virginia, 1975.

Shutko, A. M., and G. Granov, Some peculiarities of formulation and solution of inverse problems in microwave radiometry of the ocean surface and atmosphere, *IEEE J. Oceanic Eng., OE-7* (1), 40–43, 1982.

Skou, N., Airborne multifrequency radiometry of sea ice, report, Electromagn. Inst. Tech. Univ. of Denmark, Lyngby, Denmark, 1980.

(Received June 4, 1982;
revised September 7, 1982;
accepted September 8, 1982.)